



Hong, D., Hill, T. L., & Neild, S. A. (2019). Conditions for the existence of isolated backbone curves. *Proceedings of the Royal Society A: Mathematical and Physical Sciences*, 475, [0374].  
<https://doi.org/10.1098/rspa.2019.0374>

Publisher's PDF, also known as Version of record

License (if available):  
CC BY

Link to published version (if available):  
[10.1098/rspa.2019.0374](https://doi.org/10.1098/rspa.2019.0374)

[Link to publication record in Explore Bristol Research](#)  
PDF-document

This is the final published version of the article (version of record). It first appeared online via The Royal Society at <https://royalsocietypublishing.org/doi/10.1098/rspa.2019.0374> . Please refer to any applicable terms of use of the publisher.

## University of Bristol - Explore Bristol Research

### General rights

This document is made available in accordance with publisher policies. Please cite only the published version using the reference above. Full terms of use are available:  
<http://www.bristol.ac.uk/red/research-policy/pure/user-guides/ebr-terms/>

## Research



**Cite this article:** Hong D, Hill TL, Neild SA. 2019 Conditions for the existence of isolated backbone curves. *Proc. R. Soc. A* **475**: 20190374. <http://dx.doi.org/10.1098/rspa.2019.0374>

Received: 14 June 2019

Accepted: 4 November 2019

**Subject Areas:**

mechanical engineering, mathematical modelling

**Keywords:**

structural dynamics, nonlinear normal mode, backbone curves, isola, perturbation analysis

**Author for correspondence:**

Dongxiao Hong

e-mail: [dx.hong@bristol.ac.uk](mailto:dx.hong@bristol.ac.uk)

Electronic supplementary material is available online at <https://doi.org/10.6084/m9.figshare.c.4742093>.

# Conditions for the existence of isolated backbone curves

Dongxiao Hong, Thomas L. Hill and Simon A. Neild

Department of Mechanical Engineering, University of Bristol, Bristol BS8 1TR, UK

DH, 0000-0001-7861-8087; TLH, 0000-0002-4125-7895; SAN, 0000-0003-4122-4513

Isolated backbone curves represent significant dynamic responses of nonlinear systems; however, as they are disconnected from the primary responses, they are challenging to predict and compute. To explore the conditions for the existence of isolated backbone curves, a generalized two-mode system, which is representative of two extensively studied examples, is used. A symmetric two-mass oscillator is initially studied and, as has been previously observed, this exhibits a perfect bifurcation between its backbone curves. As this symmetry is broken, the bifurcation splits to form an isolated backbone curve. Here, it is demonstrated that this perfect bifurcation, indicative of a symmetric structure, may be preserved when the symmetry is broken under certain conditions; these are derived analytically. With the symmetry broken, the second example—a single-mode nonlinear structure with a nonlinear tuned mass damper—is considered. The evolution of the system's backbone curves is investigated in nonlinear parameter space. It is found that this space can be divided into several regions, within which the backbone curves share similar topological features, defining the conditions for the existence of isolated backbone curves. This allows these features to be more easily accounted for, or eliminated, when designing nonlinear systems.

## 1. Introduction

Over recent decades, demand on the performance of engineering structures has been continually growing. Meeting this demand often requires extending the performance envelope of structures to regions where

nonlinearity must be accounted for. This results in complex nonlinear dynamic phenomena, such as bifurcations, internal resonances and multiple solutions [1–6]. Despite the challenges these phenomena have posed to analysis and design, recent studies seek to exploit, rather than avoid, the nonlinear behaviours. Application areas include vibration absorbers and energy harvesting [7–13]. Among these applications, the nonlinear tuned mass damper (NLTMD) has been extensively studied in the literature with its advantageous performance demonstrated [14–17].

Den Hartog [18] proposed a widely adopted method to optimize the parameters of a linear tuned mass damper (LTMD). Later, a nonlinear generalization of Den Hartog's equal-peak method for an NLTMD was established in [16], where the performance between the NLTMD and the LTMD was compared. Gatti [17] highlights that the main advantage of introducing nonlinearity is the improvement of the bandwidth of the device. An NLTMD has, for example, been used to control a supercritical Hopf-bifurcation of aerofoil flutter in [19], and to control limit cycle oscillations of mechanical systems in [20].

Besides these favourable properties, the use of an NLTMD may bring some undesirable dynamic phenomena, such as isolas, i.e. forced responses that are isolated from the primary response branches. Due to this feature, the existence of isolas can be difficult to determine; furthermore, these isolated solutions may represent significant, high-amplitude responses [16, 21–23]. An early study of isolas in engineering systems was carried out by Abramson [24] in 1955. Extensive work since this has focused on the mechanism for their creation, such as discontinuity [25,26], internal resonances [27] and symmetry breaking [28,29].

Numerous approaches have been used to detect and trace isolas. One numerical method is continuation which uses special points, such as fold bifurcations and extremum points, to trace the evolution of isolas by varying specific parameters [30,31]. In combination with continuation methods, singularity theory can be used to provide complementary information in the prediction and identification of isolas [32–34]. Methods based on continuation can efficiently find isolas; however, they require a good understanding of the system, and its responses, to select the appropriate continuation parameters. Another numerical method is global analysis, which may detect an isola by finding initial conditions which are within the basin of attraction of that isola [35]. This approach requires a large number of simulations of initial conditions, making it computationally expensive. In addition to these methods, experimental techniques are also used to detect isolas; for example, using control-based continuation, an isola is detected for a nonlinear beam structure in [36].

An alternative approach to considering forced responses is to analyse the underlying backbone curves of the unforced, undamped system. Backbone curves, which are also known as nonlinear normal modes (NNMs), are also widely used in nonlinear modal analysis, reduced-order modelling and localization analysis (e.g. [5,6,37]). Backbone curves can be related to the forced responses of a system (including those that lie on isolas) using energy balance analysis [29,30,38]. This involves finding the points in the forced responses that lie on the backbone curves, such that the forcing energy in matches the damping energy loss. This approach reduces the isola-finding problem to an analytical and computationally simpler one; however, it requires that the backbone curves are known.

To complicate matters, while less studied than the forced counterpart, backbone curves themselves can also be isolated.<sup>1</sup> Isolated backbone curves have been demonstrated for a simple, near-symmetric two-mass oscillator [38], and it was shown that this isolated curve emerged due to the breaking of symmetry. Recently, an isolated backbone curve has also been measured experimentally for a cross-beam system using a nonlinear force appropriation technique [39], and again shown to evolve from the symmetry breaking in the system. Without *a priori* knowledge of such isolated backbone curves, any isolated forced responses that are associated with them may go undetected. While the aforementioned systems exhibit isolated backbone curves during symmetry-breaking, in practice, some systems cannot be symmetric, e.g. a grounded structure

<sup>1</sup>Note the distinction between isolated backbone curves and *isolas*, which exist in the forced responses.

with an ungrounded NLTMD attached, and the existence of isolas can have a significant impact on their performance, as discussed above. A general methodology, describing the relationship between the symmetry of the system and the evolution of isolated backbone curves, has not yet been fully explored. To understand this relationship, a more general case needs to be considered. Such insights into this relationship would ensure that isolated backbone curves can be reliably predicted when designing nonlinear devices and structures.

This paper presents a technique to determine the existence of isolated backbone curves for a two-mode system with cubic nonlinearities and a 1:1 internal resonance. This is motivated by the fact that much of the current literature on modal interactions consider systems where just two modes interact. The general two-mode model is related to two specific example systems: an in-line two-mass oscillator is used to explore the relationship between symmetry breaking and isolated backbone curves; the second motivating example is an NLTMD attached to a single-mode nonlinear structure. Exploiting the method developed for the general two-mode case, the evolution of isolated backbone curves in nonlinear parameter space is identified for the NLTMD system. To this end, the rest of this paper is organized as follows.

Section 2 firstly revisits the backbone curves of a two-mode symmetric system, which has been considered extensively (e.g. [5,29,37,38,40,41]). This system exhibits two single-mode backbone curves with one perfect bifurcation leading to mixed-mode backbone curves. By breaking the symmetry of this system, the perfect bifurcation splits to form an isolated backbone curve. It is then shown that, similarly to a symmetric system, an asymmetric system may also exhibit single-mode backbone curves with a perfect bifurcation. The mechanisms by which symmetry breaking affects the modal equations are then explored. Section 3 considers a nonlinear structure with an NLTMD and, using the insights from §2, derives the analytical parameter relationships to obtain two single-mode backbone curves with one perfect bifurcation. Perturbing the linear and nonlinear parameters from these relationships, the evolution of backbone curves in nonlinear parameter space is then discussed, and the emergence and evolution of isolated backbone curve addressed. Focusing on the system with hardening springs, discriminant analysis is used in §4 to find the analytical conditions under which the isolated backbone curve may be removed, i.e. shifted to infinite frequency and amplitude. Analytical expressions found in §§3 and 4 serve as boundaries, distinguishing topological features of backbone curves in nonlinear parameter space, and defining conditions for the existence of isolated backbone curves. Lastly, this paper is closed with conclusion in §5.

## 2. Breaking the symmetry of a nonlinear 2-d.f. oscillator

In this section, a general two-mode<sup>2</sup> conservative system, with cubic nonlinearities, is firstly considered, before considering a specific two-mode system. The Lagrangian of this general system may be written

$$\mathcal{L} = \frac{1}{2}\dot{q}_1^2 + \frac{1}{2}\dot{q}_2^2 - \frac{1}{2}\omega_{n1}^2 q_1^2 - \frac{1}{2}\omega_{n2}^2 q_2^2 - \frac{1}{4}\Psi_4 q_1^4 - \Psi_1 q_1^3 q_2 - \frac{1}{2}\Psi_3 q_1^2 q_2^2 - \Psi_2 q_1 q_2^3 - \frac{1}{4}\Psi_5 q_2^4, \quad (2.1)$$

where  $q_i$ ,  $\dot{q}_i$  and  $\omega_{ni}$  are the  $i$ th linear modal displacement, velocity and natural frequency respectively, and  $\Psi_1, \dots, \Psi_5$  are the nonlinear coefficients. Note that the nonlinear coefficients are defined in this order for simplicity in later sections. Applying the Euler–Lagrange equation then leads to the following equations of motion:

$$\ddot{q}_1 + \omega_{n1}^2 q_1 + \Psi_4 q_1^3 + 3\Psi_1 q_1^2 q_2 + \Psi_3 q_1 q_2^2 + \Psi_2 q_2^3 = 0 \quad (2.2a)$$

and

$$\ddot{q}_2 + \omega_{n2}^2 q_2 + \Psi_1 q_1^3 + \Psi_3 q_1^2 q_2 + 3\Psi_2 q_1 q_2^2 + \Psi_5 q_2^3 = 0. \quad (2.2b)$$

Note that the use of the Lagrangian in deriving these expressions restricts the number of nonlinear parameters to five, while ensuring that the equations of motion remain conservative [42,43].

<sup>2</sup>Note that the term *mode* is used here to refer to a mode of the underlying linear model of the system, whereas a *Nonlinear Normal Mode* (NNM) denotes a periodic response of the conservative nonlinear system [5].

From equation (2.2b), when the coefficient of  $q_1^3$  equals 0 (i.e. when  $\Psi_1 = 0$ ),  $q_2 = 0$  is a solution (although coupling between the two modes still exists via other terms). Substituting this into equation (2.2a) gives the single-mode solution, representing a single-mode backbone curve, or NNM branch, which consists of only the first linear modal coordinate,  $q_1$ , by solving

$$\ddot{q}_1 + \omega_{n1}^2 q_1 + \Psi_4 q_1^3 = 0. \quad (2.3)$$

Note that  $\Psi_1 = 0$  is the special case which results in this single-mode backbone, a solution which cannot exist when  $\Psi_1 \neq 0$ . In addition to this single-mode solution, backbone curves containing contributions from both linear modes, i.e. mixed-mode backbone curves, can also be found when  $\Psi_1 = 0$ . Likewise, when the coefficient of  $q_2^3$  in equation (2.2a),  $\Psi_2$ , equals 0, one can find the single-mode solution that consists of only the second linear modal coordinate,  $q_2$ , from

$$\ddot{q}_2 + \omega_{n2}^2 q_2 + \Psi_5 q_2^3 = 0. \quad (2.4)$$

Otherwise, when both  $\Psi_1 \neq 0$  and  $\Psi_2 \neq 0$ , this system only has mixed-mode backbone curves. To find the backbone curves of the general two-mode system, the harmonic balance technique<sup>3</sup> is used, firstly by assuming that the modal displacements may be written as

$$q_i \approx u_i = U_i \cos(\omega_{ri}t - \theta_i), \quad (2.5)$$

where  $u_i$  represents the fundamental response of  $q_i$ , and where  $U_i$ ,  $\omega_{ri}$  and  $\theta_i$  are amplitude, response frequency and phase of  $u_i$ , respectively. Note that this trigonometric solution is equivalent to the exponential form used in [38,41]. It is further assumed that the fundamental frequencies of the two modes are equal, i.e.  $\omega_{r1} = \omega_{r2} = \Omega$ , hence, the response frequency ratio is 1:1. With the substitution of expressions (2.5) into the equations of motion (2.2), and the non-resonant terms removed, one can obtain the time-independent solutions from

$$4(\omega_{n1}^2 - \Omega^2)U_1 + 3\Psi_4 U_1^3 + \Psi_3 U_1 U_2^2 [1 + 2\cos^2(\theta_d)] + 3(\Psi_2 U_2^3 + 3\Psi_1 U_1^2 U_2) \cos(\theta_d) = 0, \quad (2.6a)$$

$$4(\omega_{n2}^2 - \Omega^2)U_2 + 3\Psi_5 U_2^3 + \Psi_3 U_1^2 U_2 [1 + 2\cos^2(\theta_d)] + 3(\Psi_1 U_1^3 + 3\Psi_2 U_1 U_2^2) \cos(\theta_d) = 0 \quad (2.6b)$$

$$\text{and } [2\Psi_3 U_1 U_2 \cos(\theta_d) + 3\Psi_1 U_1^2 + 3\Psi_2 U_2^2] \sin(\theta_d) = 0, \quad (2.6c)$$

where  $\theta_d = \theta_1 - \theta_2$ . These equations can then be used to compute the backbone curves of the general two-mode system.

### (a) The backbone curves of a symmetric two-mass oscillator

To demonstrate the effect of symmetry breaking, a specific two-mode system, the two-mass oscillator shown schematically in figure 1, is now used. The system consists of two masses with mass values  $m_1$  and  $m_2$ , and displacements  $x_1$  and  $x_2$ , respectively. These masses are grounded via two linear springs, with coefficients  $k_1$  and  $k_3$ , respectively, and are connected by another linear spring with coefficient  $k_2$ . This system also contains three nonlinear cubic springs with coefficients  $\alpha_1$ ,  $\alpha_2$  and  $\alpha_3$ , as shown in figure 1. The backbone curves of this system can be computed from equations (2.6), using the relationship between the nonlinear modal coefficients,  $\Psi_i$ , and the physical parameters of the model, as derived in appendix A.

Here, the symmetry of the system is divided into two parts: linear symmetry (LS), where both  $m_1 = m_2$  and  $k_1 = k_3$ ; and nonlinear symmetry (NS), where  $\alpha_1 = \alpha_3$ . Note that the LS–NS case leads to  $\Psi_1 = 0$  and  $\Psi_2 = 0$ , as shown in appendix A—see equation (A 9) with  $\alpha_1 = \alpha_3$ . As previously discussed, this leads to single-mode solutions. The backbone curves of the system with both LS and NS have been investigated in detail in [29,38,41], and an example is illustrated in

<sup>3</sup>Other analytical methods, such as the second-order normal form technique [44] or the multiple-scales method [45], could alternatively be used.

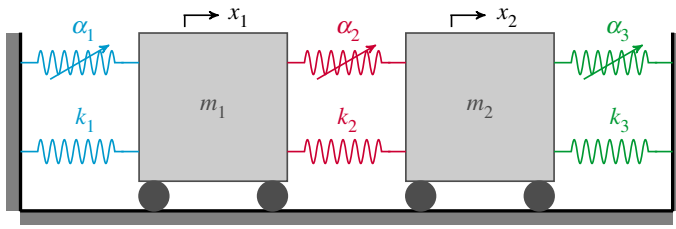


**Figure 1.** A schematic diagram of a two-mode system in the form of a two-mass oscillator. Two masses, with mass values  $m_1$  and  $m_2$ , have displacements  $x_1$  and  $x_2$ , respectively, while linear and nonlinear cubic springs have coefficients  $k_i$  and  $\alpha_i$ , respectively, where  $i = 1, 2, 3$ . (Online version in colour.)

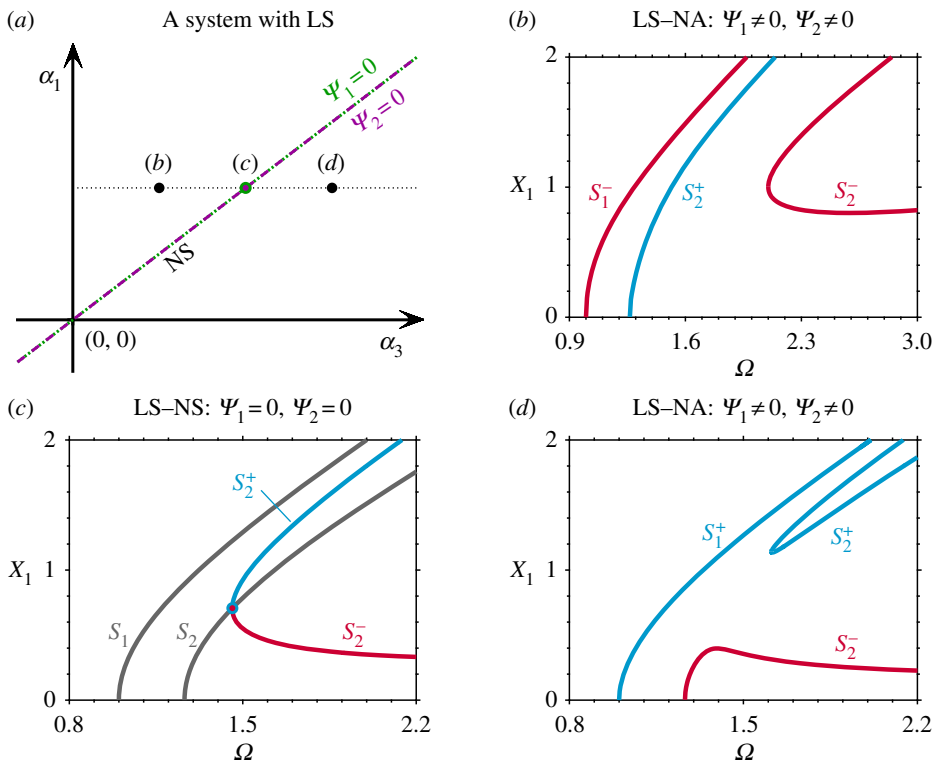


**Figure 2.** The effect of breaking the nonlinear symmetry (NS), i.e. breaking the condition  $\alpha_1 = \alpha_3$ , for a system with linear symmetry (LS), i.e.  $m_1 = m_2$  and  $k_1 = k_3$ . (a) The nonlinear parameter space,  $\alpha_1$  against  $\alpha_3$ , for the system with LS when  $m_1 = m_2 = 1$ ,  $k_1 = k_3 = 1$ ,  $k_2 = 0.3$  and  $\alpha_2 = 0.05$ . The  $\alpha_1$  and  $\alpha_3$  values that lead to  $\Psi_1 = 0$  and  $\Psi_2 = 0$  are shown as a green dotted line and a purple dashed line, respectively. (b) Backbone curves for a system with linear symmetry and nonlinear asymmetry (NA) when  $\alpha_1 = 1$ ,  $\alpha_3 = 0.5$  (represented by a black dot labelled (b) in panel (a)). (c) Backbone curves for an LS–NS system with  $\alpha_1 = 1$ ,  $\alpha_3 = 1$ , where the solid point represents the perfect bifurcation (denoted by a solid dot labelled (c) in panel (a)). (d) Backbone curves for an LS–NA system with  $\alpha_1 = 1$ ,  $\alpha_3 = 1.5$  (represented by a black dot labelled (d) in panel (a)). Panels (b)–(d) are shown in the projection of the response frequency,  $\Omega$ , against the amplitude of the first mass,  $X_1$ . (Online version in colour.)

figure 2c. The single-mode backbone curves  $S_1$  and  $S_2$  consist of only the first and second modal coordinates, respectively; while  $S_2^+$  and  $S_2^-$  represent mixed-mode backbone curves containing both linear modal coordinates. The subscripts of  $S_2^+$  and  $S_2^-$  indicate the backbone curve from which they bifurcate (i.e. from  $S_2$  in this case), and the superscripts  $+$  and  $-$  denote in-phase and anti-phase responses between the fundamental components of the linear modal coordinates,

respectively. For details of how these backbone curves have been computed, using equations (2.6), see [29,38,41].

Here, we introduce the concept of *dynamic symmetry* to describe backbone curves with the features of an LS–NS system, specifically characterized by the following features:

- (i) two single-mode backbone curves,  $S_1$  and  $S_2$ .
- (ii) two mixed-mode backbone curves; either  $S_2^\pm$ , emerging from a perfect bifurcation on  $S_2$ , or  $S_1^\pm$ , emerging from a perfect bifurcation on  $S_1$ .

### (b) Breaking **either** the nonlinear **or** the linear parameter symmetry

Figure 2a represents the nonlinear parameter space of  $\alpha_1$  against  $\alpha_3$ —i.e. the parameters of the two nonlinear grounding springs—for the case where the system has LS. The nonlinear parameters leading to  $\Psi_1 = 0$  and  $\Psi_2 = 0$  are denoted by green dotted and purple dashed lines, respectively. In this case, i.e. for LS, these lines correspond to NS. In other words, for this simple system, both LS and NS will always lead to  $\Psi_1 = \Psi_2 = 0$ , hence resulting in single-mode backbone curves which is one of the conditions for dynamic symmetry. For nonlinear parameter combinations with nonlinear asymmetry (NA), i.e.  $\alpha_1 \neq \alpha_3$ , both  $\Psi_1 \neq 0$  and  $\Psi_2 \neq 0$ , as indicated by the dots labelled (b) and (d) in figure 2a. This symmetry breaking turns the single-mode backbone curves into mixed-mode ones, breaks the perfect bifurcation, and generates an isolated backbone curve. As shown in figure 2b,d (corresponding to parameters labelled (b) and (d) in figure 2a), an isolated backbone curve emerges from two primary mixed-mode backbone curves, as observed in [29]. As proven in appendix A, a system with LS and NA cannot exhibit dynamic symmetry as in this case  $\Psi_1 \neq 0$  and  $\Psi_2 \neq 0$ .

Similarly, breaking the LS, while retaining the NS, can also break the dynamic symmetry. With the breaking of the LS ( $m_2 = 0.8m_1$  and  $k_3 = 0.7k_1$ ), the orientations of  $\Psi_1 = 0$  and  $\Psi_2 = 0$  are changed, and are no longer overlapping, as shown in figure 3a. If the NS is retained, i.e.  $\alpha_1 = \alpha_3$  (depicted by the grey line in figure 3a), the backbone curves, depicted in figure 3b, are similar in form to the ones for the LS–NA system in figure 2d, i.e. one isolated backbone curve between two primary mixed-mode backbone curves. The LA–NS system considered here cannot have dynamic symmetry since the intersection of  $\Psi_1 = 0$  and  $\Psi_2 = 0$ , where one can find two single-mode backbone curves, is not on the line representing  $\alpha_1 = \alpha_3$  (i.e. the point at which the green and purple lines in figure 3a cross does not correspond to the grey line).

### (c) Breaking **both** the linear **and** nonlinear parameter symmetry

Following from the LA–NS system considered in §2b, the NS is also broken to investigate the backbone curves of an LA–NA system. Figure 4b shows the backbone curves for the case where  $\alpha_3$  is reduced from the NS-case to the point where  $\Psi_2 = 0$ , marked as a purple dot labelled (b) in figure 4a. As expected, this leads to a single-mode backbone curve  $S_2$ ; however, as  $\Psi_1 \neq 0$ , the first primary backbone curve,  $S_1^+$ , contains a component of the second mode with in-phase modal coordinates. As such, this is not a dynamically symmetric case, despite sharing some characteristics, such as the backbone curves  $S_2^+$  and  $S_2^-$  which bifurcate off  $S_2$ . Further reducing  $\alpha_3$  leads to the point where  $\Psi_1 = 0$ , shown as a green dot labelled (c) in figure 4a, whose backbone curves are shown in figure 4c. These exhibit a single-mode backbone curve  $S_1$  (as predicted by the  $\Psi_1 = 0$  condition) but with a primary and an isolated backbone curve,  $S_2^+$  and  $S_2^-$ . As shown in figure 4a,  $\Psi_1 = \Psi_2 = 0$  may still be satisfied for this case if  $\alpha_1$  and  $\alpha_3$  are on the intersection of  $\Psi_1 = 0$  and  $\Psi_2 = 0$ , i.e. the point labelled (d) in figure 4a. Dynamic symmetry can therefore be obtained for such an LA–NA system, as can be seen from the backbone curves in figure 4d.

As previously discussed, the concept of dynamic symmetry is defined as having similar characteristics to an LS–NS system; nonetheless, such behaviour can be observed in an LA–NA system, if parameters are appropriately selected. This means that an LA–NA system can exhibit the same dynamic characteristics as a fully symmetric system. Furthermore, defining conditions

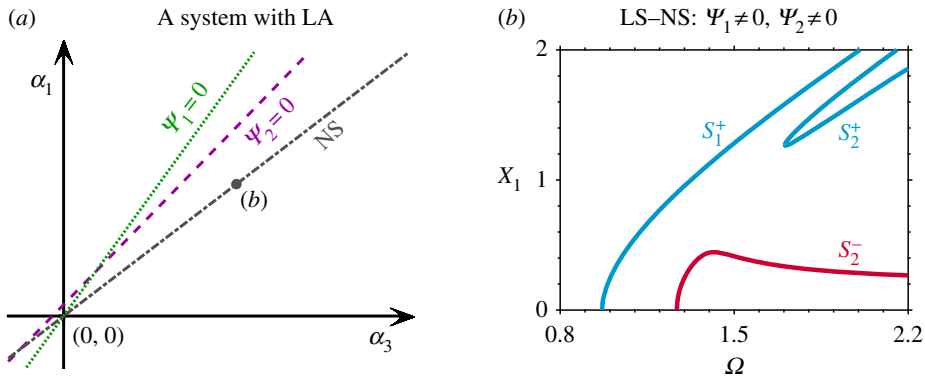


**Figure 3.** The effect of breaking the linear symmetry (LS) for a system with nonlinear symmetry (NS). (a) The nonlinear parameter space for the system with linear asymmetry (LA) when  $m_1 = 1$ ,  $m_2 = 0.8$ ,  $k_1 = 1$ ,  $k_3 = 0.7$ ,  $k_2 = 0.3$  and  $\alpha_2 = 0.05$ . The  $\alpha_1$  and  $\alpha_3$  values that lead to  $\Psi_1 = 0$  and  $\Psi_2 = 0$  are shown as a green dotted line and a purple dashed line, respectively, and parameters leading to NS are shown as a dash-dotted grey line. (b) Backbone curves for an LA–NS system with  $\alpha_1 = 1$ ,  $\alpha_3 = 1$  (represented by a grey dot labelled (b) in panel (a)) in the projection of the response frequency,  $\Omega$ , against the amplitude of the first mass,  $X_1$ . (Online version in colour.)

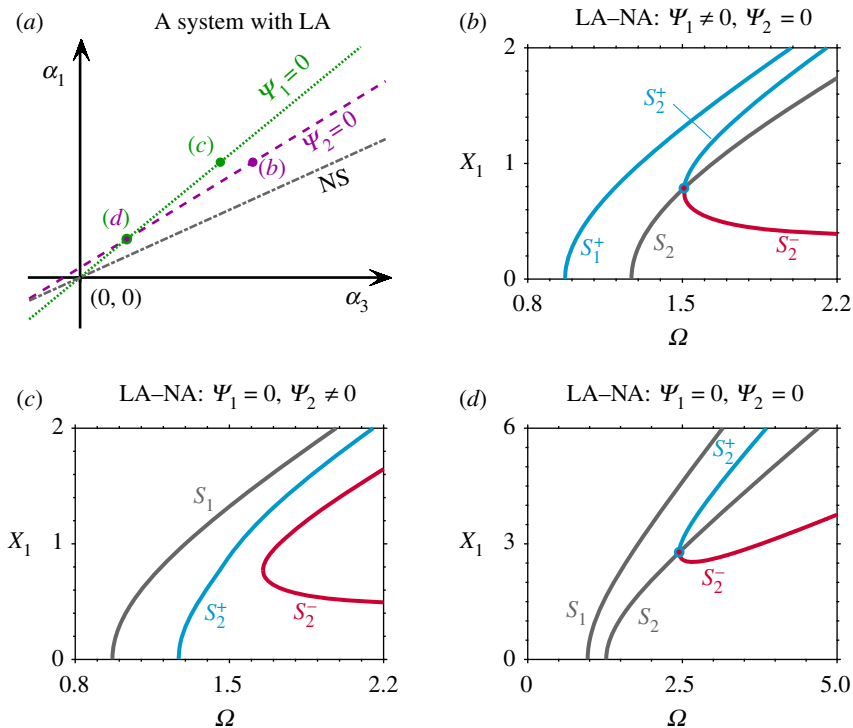


**Figure 4.** Obtaining dynamic symmetry for an LA–NA system. (a) The nonlinear parameter space for a system with LA (linear parameters and  $\alpha_2$  are equal to those considered in figure 3). The  $\alpha_1$  and  $\alpha_3$  values that lead to  $\Psi_1 = 0$  and  $\Psi_2 = 0$  are shown as a green-dotted and a purple-dashed lines, respectively, and parameters leading to NS are shown as a dash-dotted grey line. (b) Backbone curves for an LA–NA system with  $\alpha_1 = 1$ ,  $\alpha_3 \approx 0.6785$  (represented by a purple dot labelled (b) in panel (a)). (c) Backbone curves for an LA–NA system with  $\alpha_1 = 1$ ,  $\alpha_3 \approx 0.5510$  (denoted by a green dot labelled (c) in panel (a)). (d) Backbone curves for an LA–NA system with  $\alpha_1 \approx 0.3333$ ,  $\alpha_3 \approx 0.1833$  (represented by a solid dot labelled (d) in panel (a)). (Online version in colour.)



for the existence of single-mode solutions, expressions  $\Psi_1 = 0$  and  $\Psi_2 = 0$  also serve as boundaries, which divide the nonlinear parameter space into several regions, within which the backbone curves share similar topological features. These regions, in the nonlinear parameter space, allow the changes in the fundamental dynamic behaviours to be identified and predicted.

### 3. Backbone curves for an NLTMD-inspired two-mode system

In this section, a two-mode asymmetric system, depicted in figure 5, is considered. This system is equivalent to that shown in figure 1, but with the springs grounding the second mass removed. This system is representative of a nonlinear structure (first mass) with an NLTMD (second mass) attached.

Isolated backbone curves represent particularly undesirable features in an NLTMD device [16,21,23], due to the difficulty of predicting them, and their potential to represent high-amplitude dynamic responses. To further understand their features, in this section the parameter conditions required for dynamic symmetry are first found. However, in practice, the optimized linear parameters of an NLTMD cannot usually satisfy such conditions. The evolution of backbone curves in nonlinear parameter space, for an optimized set of linear parameters, is then investigated and used to determine the conditions for the existence of isolated backbone curves.

#### (a) Parameter conditions required for dynamic symmetry

As discussed in §2, an LA–NA system can exhibit dynamic symmetry if the parameters are selected appropriately. One feature of dynamic symmetry is having two single-mode solutions,  $S_1$  and  $S_2$ , which requires that both  $\Psi_1 = 0$  and  $\Psi_2 = 0$  in the equations of motion (2.2). The expressions of  $\Psi_1$  and  $\Psi_2$  for the NLTMD system are given in equations (A 5), and may be written in matrix form as

$$\begin{pmatrix} \Psi_1 \\ \Psi_2 \end{pmatrix} = \begin{bmatrix} \phi_{11}^3 \phi_{12} & (\phi_{11} - \phi_{21})^3 (\phi_{12} - \phi_{22}) \\ \phi_{11} \phi_{12}^3 & (\phi_{11} - \phi_{21}) (\phi_{12} - \phi_{22})^3 \end{bmatrix} \begin{pmatrix} \alpha_1 \\ \alpha_2 \end{pmatrix}, \quad (3.1)$$

where  $\alpha_3 = 0$  has been substituted (i.e. no nonlinear spring grounding the second mass) and where  $\phi_{ij}$  are elements of the linear modeshape matrix  $\Phi$ , defined as

$$\Phi = \begin{bmatrix} \phi_{11} & \phi_{12} \\ \phi_{21} & \phi_{22} \end{bmatrix}. \quad (3.2)$$

Note that the first column of this matrix, i.e.  $\phi_{11}$  and  $\phi_{21}$ , represents the modeshape of the first linear mode, while the second linear modeshape is captured by  $\phi_{12}$  and  $\phi_{22}$ , in the second column of  $\Phi$ . In order for  $\Psi_1 = 0$  and  $\Psi_2 = 0$  to be satisfied, equation (3.1) shows that either  $\alpha_1 = 0$  and  $\alpha_2 = 0$  (which would represent the trivial case where the system is linear), or that the determinant of the matrix in equation (3.1) must be zero, i.e.

$$\phi_{11}^3 \phi_{12} (\phi_{11} - \phi_{21}) (\phi_{12} - \phi_{22})^3 - \phi_{11} \phi_{12}^3 (\phi_{11} - \phi_{21})^3 (\phi_{12} - \phi_{22}) = 0. \quad (3.3)$$

Note that for a system with an asymmetric configuration,  $\phi_{ij}$  are non-zero, and  $\phi_{11} \neq \phi_{21}$  and  $\phi_{12} \neq \phi_{22}$ . Thus, equation (3.3) can be rearranged to

$$\frac{\phi_{11}^2 (\phi_{12} - \phi_{22})^2}{\phi_{12}^2 (\phi_{11} - \phi_{21})^2} = 1, \quad (3.4)$$

which can be satisfied using the following conditions:

$$\frac{\phi_{11} (\phi_{12} - \phi_{22})}{\phi_{12} (\phi_{11} - \phi_{21})} = 1: \quad \frac{\phi_{11}}{\phi_{21}} - \frac{\phi_{12}}{\phi_{22}} = 0 \quad (3.5a)$$

and

$$\frac{\phi_{11} (\phi_{12} - \phi_{22})}{\phi_{12} (\phi_{11} - \phi_{21})} = -1: \quad \frac{\phi_{21}}{\phi_{11}} + \frac{\phi_{22}}{\phi_{12}} = 2. \quad (3.5b)$$

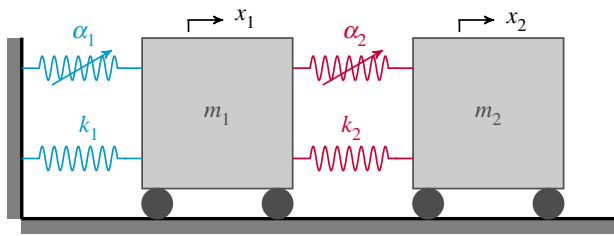


**Figure 5.** A schematic diagram of a two-mode asymmetric system, representative of a nonlinear structure with an NLMD. (Online version in colour.)

Condition (3.5a) cannot be satisfied as it requires that the first and second modeshapes are equal; therefore, dynamic symmetry, i.e. when  $\Psi_1 = \Psi_2 = 0$ , may only be achieved when condition (3.5b) is satisfied. The relationship between the modeshape coefficients,  $\phi_{ij}$ , and the linear physical parameters is derived in appendix A. Substituting equations (A 7) into condition (3.5b) (also using equation (A 6)) leads to

$$\frac{k_1}{k_2} = \frac{m_1 + m_2}{m_2}. \quad (3.6)$$

This demonstrates that, in order for the NLMD-inspired system to exhibit dynamic symmetry, the linear stiffness coefficients must obey the ratio described by equation (3.6). As well as this condition for the linear parameters, the relationship between the nonlinear parameters may be found by substituting expressions (3.6) and (A 7) back into equation (3.1), leading to

$$\frac{\alpha_1}{\alpha_2} = \frac{(\phi_{12} - \phi_{22})^4}{\phi_{12}^4} = \frac{(\phi_{11} - \phi_{21})^4}{\phi_{11}^4} = \left(\frac{m_1 + m_2}{m_2}\right)^2. \quad (3.7)$$

Figure 6a shows the nonlinear parameter space  $\alpha_1$  against  $\alpha_2$ , for the case where  $k_1/k_2 = 21$ , and where the mass values satisfy equation (3.6). The overlapping green and purple lines represent the parameter relationships that lead to  $\Psi_1 = 0$  and  $\Psi_2 = 0$ , respectively (in this instance the case  $\alpha_1/\alpha_2 = 441$ , satisfies equation (3.7) and hence  $\Psi_1 = \Psi_2 = 0$ ). Despite being a linearly asymmetric system, this has strong similarities to figure 2a, which represents an LS system, and indicates that multiple nonlinear parameter combinations will lead to dynamic symmetry. Note that when the parameter relationships (3.6) and (3.7) are satisfied, expressions for  $\Psi_1, \dots, \Psi_5$  (A 5) can be simplified as

$$\Psi_1 = 0, \quad \Psi_2 = 0, \quad \Psi_3 = 6\phi_{11}^2\phi_{12}^2\alpha_1, \quad \Psi_4 = 2\phi_{11}^4\alpha_1, \quad \Psi_5 = 2\phi_{12}^4\alpha_1. \quad (3.8)$$

With  $\Psi_1 = 0$  and  $\Psi_2 = 0$ , expressions for backbone curves (2.6) can be reduced to

$$\left\{ 4(\omega_{n1}^2 - \Omega^2) + 3\Psi_4 U_1^2 + \Psi_3 U_2^2 [1 + 2\cos^2(\theta_d)] \right\} U_1 = 0, \quad (3.9a)$$

$$\left\{ 4(\omega_{n2}^2 - \Omega^2) + 3\Psi_5 U_2^2 + \Psi_3 U_1^2 [1 + 2\cos^2(\theta_d)] \right\} U_2 = 0 \quad (3.9b)$$

and 
$$2\Psi_3 U_1 U_2 \cos(\theta_d) \sin(\theta_d) = 0. \quad (3.9c)$$

The case where  $U_1 = 0$  and  $U_2 = 0$  represent the trivial case where the system is stationary. Two sets of single-mode solutions, denoted  $S_1$  and  $S_2$ , can be found with frequency–amplitude relationships described as

$$S_1: \quad U_2 = 0, \quad \Omega^2 = \omega_{n1}^2 + \frac{3}{4}\Psi_4 U_1^2 \quad (3.10)$$

and

$$S_2: \quad U_1 = 0, \quad \Omega^2 = \omega_{n2}^2 + \frac{3}{4}\Psi_5 U_2^2. \quad (3.11)$$

This system can also exhibit mixed-mode backbone curves. To compute these, the phase relationship,  $\theta_d$ , between the fundamental components of the two modal coordinates,  $u_1$  and  $u_2$ , needs to be determined. From equation (3.9c), this may be satisfied when  $\theta_d = n\pi/2$ , with  $n \in \mathbb{Z}$ . The case where  $n$  is odd, which satisfies  $\cos(\theta_d) = 0$ , represents solutions exhibiting out-of-unison

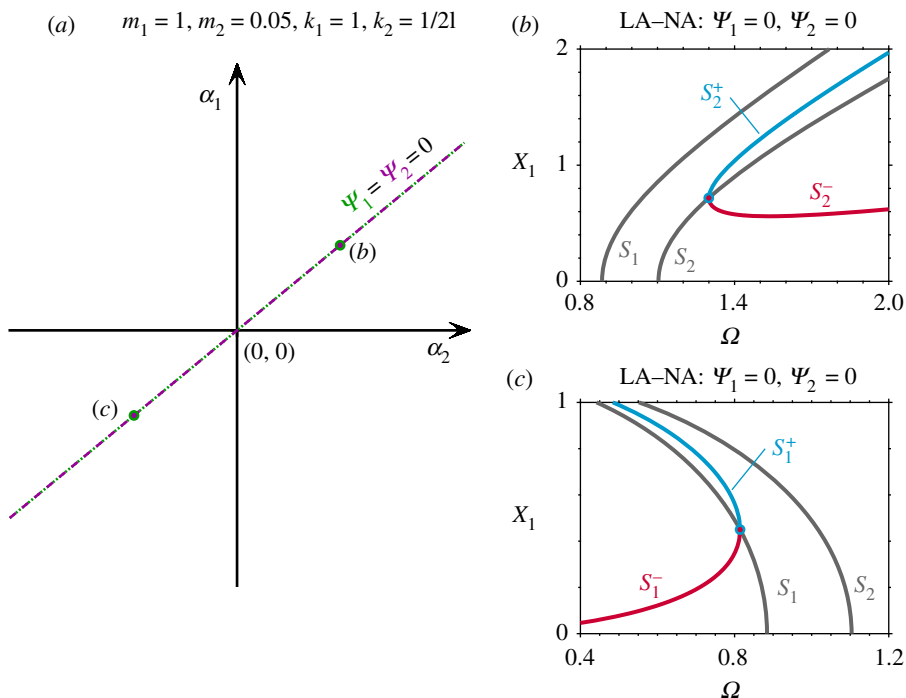


**Figure 6.** Dynamic symmetry for an NLTD-inspired system. (a) The nonlinear parameter space,  $\alpha_1$  against  $\alpha_2$ , for a system with LA, i.e.  $m_1 = 1$ ,  $m_2 = 0.05$ ,  $k_1 = 1$  and  $k_2 = 1/21$ , where  $\Psi_1 = 0$  and  $\Psi_2 = 0$  are two overlapping lines. (b) Backbone curves with dynamic symmetry for a hardening LA–NA system when  $\alpha_1 = 1$  and  $\alpha_2 = 1/441$  (represented by a solid dot labelled (b) in panel (a)). (c) Backbone curves with dynamic symmetry for a softening LA–NA system when  $\alpha_1 = -1$  and  $\alpha_2 = -1/441$  (represented by a solid dot labelled (c) in panel (a)). (Online version in colour.)

resonance [46], i.e. the two modes are  $\pm 90^\circ$  out-of-phase. The case where  $n$  is even, satisfying  $\sin(\theta_d) = 0$ , represents in-phase and anti-phase solutions. Considering the out-of-unison solutions, the substitution of  $\cos(\theta_d) = 0$  into equations (3.9a) and (3.9b), leads to the frequency–amplitude relationship

$$S_{1,2}^{\pm 90}: U_1^2 = \frac{4(\omega_{n2}^2 - \omega_{n1}^2) + (3\Psi_5 - \Psi_3)U_2^2}{3\Psi_4 - \Psi_3} \quad (3.12a)$$

and

$$\Omega^2 = \frac{4(3\Psi_4\omega_{n2}^2 - \Psi_3\omega_{n1}^2) + (9\Psi_4\Psi_5 - \Psi_3^2)U_2^2}{4(3\Psi_4 - \Psi_3)}. \quad (3.12b)$$

With substitution of expressions (3.6), (3.8), (A 6) and (A 8) into equation (3.12b), one can find that the response frequency,  $\Omega$ , of out-of-unison resonance, in this case, is always zero. This means that out-of-unison solutions cannot exist in the dynamically symmetric case for this system.

The in-phase solutions, corresponding to  $\theta_d = 0$  are denoted  $S_1^+$  and  $S_2^+$ , while the anti-phase solutions, corresponding to  $\theta_d = \pi$  are denoted  $S_1^-$  and  $S_2^-$  ( $S_{1,2}^\pm$  is used to denote all of them). For the dynamically symmetric case, these backbone curves all share the frequency–amplitude relationship, given by

$$S_{1,2}^\pm: U_1^2 = \frac{4(\omega_{n2}^2 - \omega_{n1}^2) + 3(\Psi_5 - \Psi_3)U_2^2}{3(\Psi_4 - \Psi_3)} \quad (3.13a)$$

and

$$\Omega^2 = \frac{4(\Psi_4\omega_{n2}^2 - \Psi_3\omega_{n1}^2) + 3(\Psi_4\Psi_5 - \Psi_3^2)U_2^2}{4(\Psi_4 - \Psi_3)}. \quad (3.13b)$$

As well as two single-mode backbone curves, described by equations (3.10) and (3.11), dynamic symmetry also requires two mixed-mode backbone curves, described by equations

(3.13), with a perfect bifurcation on either  $S_2$ , which are denoted  $S_2^\pm$ , or on  $S_1$ , which are denoted  $S_1^\pm$ . For the perfect bifurcation point on  $S_2$ , the amplitude of the first modal coordinate  $U_1 = 0$ ; likewise, the second modal amplitude  $U_2 = 0$  for the perfect bifurcation point on  $S_1$ . Using these conditions, the amplitude and frequency of these two bifurcation points can be obtained, from equations (3.13), as

$$\text{bifurcation point on } S_1: \quad U_1^2 = \frac{4(\omega_{n2}^2 - \omega_{n1}^2)}{3(\Psi_4 - \Psi_3)}, \quad \Omega^2 = \frac{\Psi_4\omega_{n2}^2 - \Psi_3\omega_{n1}^2}{\Psi_4 - \Psi_3} \quad (3.14a)$$

and

$$\text{bifurcation point on } S_2: \quad U_2^2 = \frac{4(\omega_{n2}^2 - \omega_{n1}^2)}{3(\Psi_3 - \Psi_5)}, \quad \Omega^2 = \frac{\Psi_3\omega_{n2}^2 - \Psi_5\omega_{n1}^2}{\Psi_3 - \Psi_5}. \quad (3.14b)$$

As  $\omega_{n2} > \omega_{n1}$ , to obtain positive solutions, i.e. positive amplitude and frequency, requires

$$\text{bifurcation point on } S_1: \quad \Psi_4 - \Psi_3 > 0, \quad \Psi_4\omega_{n2}^2 - \Psi_3\omega_{n1}^2 > 0 \quad (3.15a)$$

and

$$\text{bifurcation point on } S_2: \quad \Psi_3 - \Psi_5 > 0, \quad \Psi_3\omega_{n2}^2 - \Psi_5\omega_{n1}^2 > 0. \quad (3.15b)$$

Note that conditions (3.15) are valid for any system with cubic nonlinearities and a 1:1 resonance between two modes. To relate these to the NLTMD system, the expressions for modeshape elements (A 8) and the nonlinear parameter relationship (3.7) are substituted into these inequalities. This reveals that a perfect bifurcation from  $S_1$  onto  $S_1^\pm$  exists when both nonlinear parameters are softening, i.e.  $\alpha_1 < 0$  and  $\alpha_2 < 0$ ; while a perfect bifurcation from  $S_2$  onto  $S_2^\pm$  may be seen for hardening nonlinear parameters, i.e.  $\alpha_1 > 0$  and  $\alpha_2 > 0$  when  $m_2 < m_1/3$ . Figure 6*b,c* shows the backbone curves with dynamic symmetry, i.e. satisfying parameter conditions (3.6), (3.7) and (3.15) for systems with hardening and softening parameters, respectively (labelled with (b) and (c), respectively, in figure 6*a*).

## (b) Evolution of backbone curves in the nonlinear parameter space

In the previous discussion, we did not consider the tuning of the NLTMD, but rather concentrated on whether a solution exists that exhibits dynamic symmetry and derived the linear and nonlinear parameter relationships, (3.6), (3.7) and (3.15) for this to occur. Now, to investigate the evolution of backbone curves in nonlinear parameter space, it is assumed that the linear parameters of the NLTMD are tuned to achieve optimal performance.

The classical approach for optimizing the linear parameters of a TMD is known as the fixed-points method [18]. Instead of imposing two fixed points, using  $H_\infty$  optimization, a closed-form exact solution to obtain equal peaks in receptance curves of the underlying linear system is discussed in [47], where the linear stiffness of the NLTMD can be optimized using

$$k_2^{\text{opt}} = \frac{8\mu k_1 [16 + 23\mu + 9\mu^2 + 2(2 + \mu)\sqrt{4 + 3\mu}]}{3(1 + \mu)^2(64 + 80\mu + 27\mu^2)}, \quad (3.16)$$

where  $\mu = m_2/m_1$  is the mass ratio and  $k_2^{\text{opt}}$  is the optimized linear spring coefficient of the NLTMD. This cannot satisfy relationship (3.6), and hence dynamic symmetry cannot be achieved. However, if nonlinear parameters are correspondingly selected on either  $\Psi_1 = 0$  or  $\Psi_2 = 0$ , single-mode backbone curves,  $S_1$  and  $S_2$ , respectively, can still be solved via amplitude–frequency relationships (3.10) and (3.11). To find the nonlinear parameter conditions that lead to either  $\Psi_1 = 0$  or  $\Psi_2 = 0$ , the modeshape expressions (A 7) are substituted into the expressions for  $\Psi_i$  (A 5) (with  $\alpha_3 = 0$ ). Letting  $\Psi_1 = 0$  and  $\Psi_2 = 0$ , respectively, one has

$$\Psi_1 = 0: \quad \frac{\alpha_1}{\alpha_2} = -\frac{(-\omega_{n1}^2 m_1 + k_1)^3 (-\omega_{n2}^2 m_1 + k_1)}{k_2^4} \quad (3.17a)$$

and

$$\Psi_2 = 0: \quad \frac{\alpha_1}{\alpha_2} = -\frac{(-\omega_{n1}^2 m_1 + k_1) (-\omega_{n2}^2 m_1 + k_1)^3}{k_2^4}. \quad (3.17b)$$

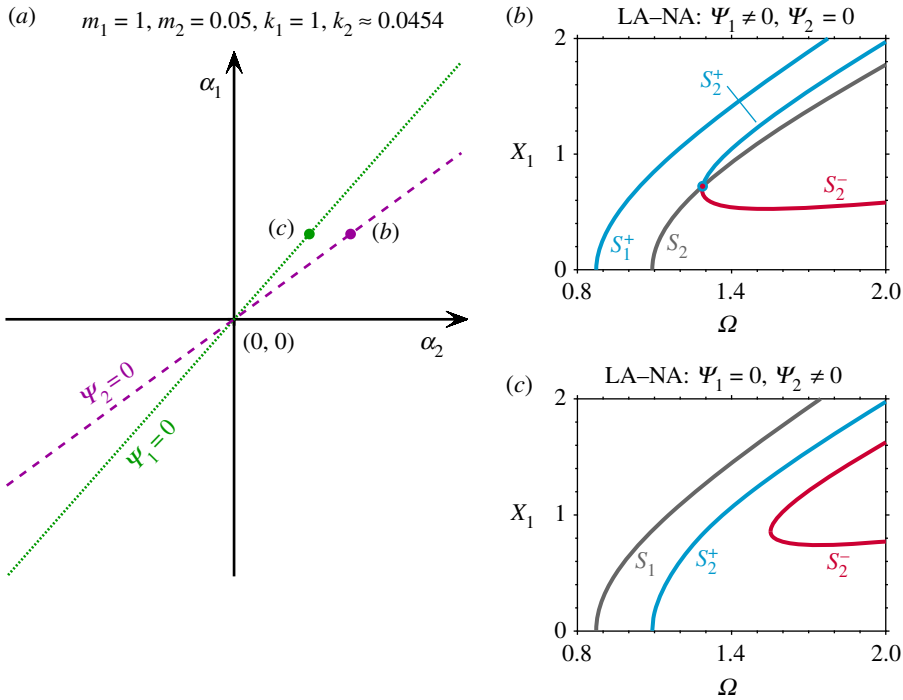


**Figure 7.** Optimizing the linear parameters of the NLTMD leads to the breaking of dynamic symmetry for an NLTMD-inspired system. (a) Nonlinear parameter space,  $\alpha_1$  against  $\alpha_2$ , for a system with LA, i.e.  $m_1 = 1, m_2 = 0.05, k_1 = 1$  and  $k_2 = k_2^{\text{opt}} \approx 0.0454$ . The  $\alpha_1$  and  $\alpha_3$  values that lead to  $\Psi_1 = 0$  and  $\Psi_2 = 0$  are shown as a green dotted line and a purple dashed line, respectively, and curves  $\Psi_1 = 0$  and  $\Psi_2 = 0$  are intersecting at the origin. (b) Backbone curves with the single-mode solution  $S_2$  for the LA–NA system when  $\alpha_1 = 1$  and  $\alpha_2 \approx 0.00256$  (represented by a purple dot labelled (b) in panel (a)). (c) Backbone curves with the single-mode backbone curve  $S_1$  for the LA–NA system when  $\alpha_1 = 1$  and  $\alpha_2 \approx 0.00166$  (represented by a green dot labelled (c) in panel (a)). (Online version in colour.)

As depicted in figure 7a, the curves  $\Psi_1 = 0$  and  $\Psi_2 = 0$  do not overlap, instead, these curves now are intersecting at the origin in the nonlinear parameter space (where the system is reduced to a linear one). Backbone curves for the system with  $\Psi_1 = 0$  and  $\Psi_2 \neq 0$  (the point labelled (c) in figure 7a) are shown in figure 7c; these are similar to those shown in figure 4c, where a single-mode backbone curve  $S_1$  is also present. Likewise, backbone curves for the system with  $\Psi_2 = 0$  and  $\Psi_1 \neq 0$  (the point labelled (b) in figure 7a) are shown in figure 7b, which have similarity to figure 4b.

Systems with nonlinear parameters that do not lie on  $\Psi_1 = 0$  or  $\Psi_2 = 0$  exhibit mixed-mode backbone curves. As previously, the phase relationship between the two modal coordinates needs to be determined using equation (2.6c). This expression is satisfied with real and positive solutions by  $\sin(\theta_d) = 0$ , leading to the phase relationship  $\theta_d = \theta_1 - \theta_2 = n\pi$ , where even and odd  $n$  values denote in-phase and anti-phase modal relationships, respectively. Further defining the phase parameter  $p$  as

$$p = \cos(\theta_d) = \cos(n\pi) = \begin{cases} +1 & \text{for even } n \\ -1 & \text{for odd } n, \end{cases} \quad (3.18)$$

allows the expressions governing the modal amplitudes and frequencies, given in (2.6a,b), to be written

$$4(\omega_{n1}^2 - \Omega^2)U_1 + 3[\Psi_4 U_1^3 + \Psi_3 U_1 U_2^2 + p(\Psi_2 U_2^3 + 3\Psi_1 U_1^2 U_2)] = 0 \quad (3.19a)$$

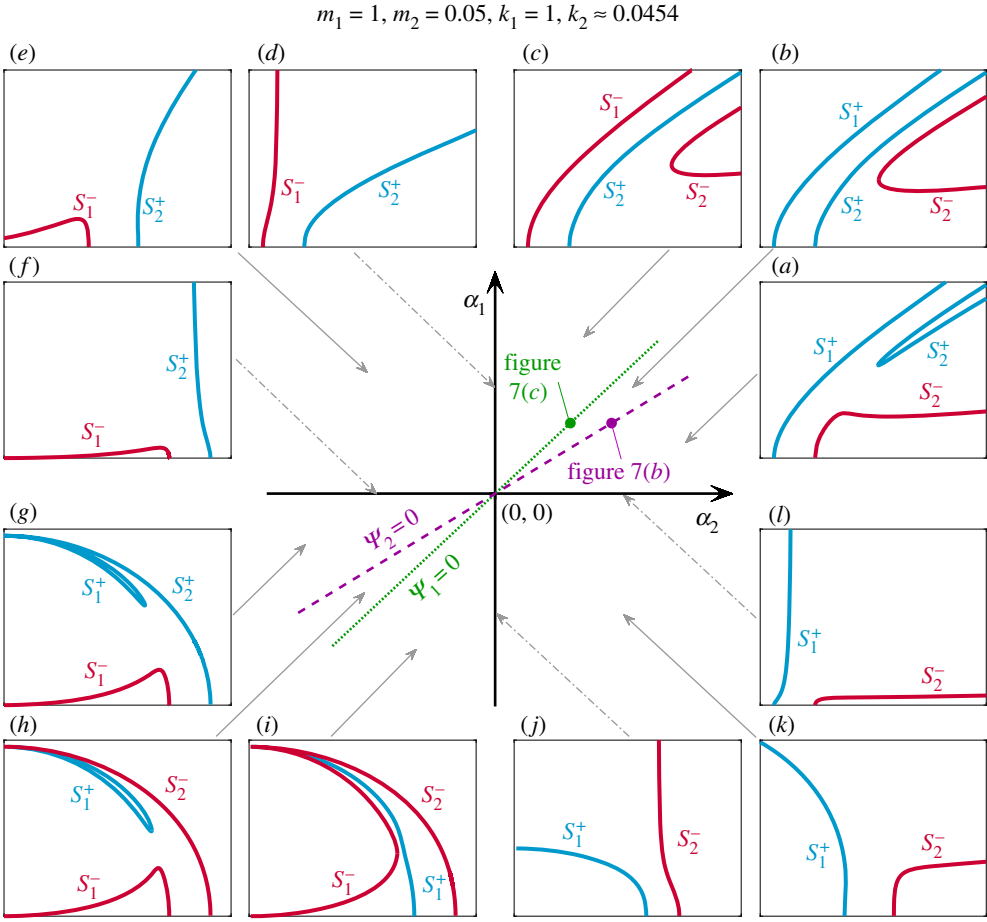


**Figure 8.** The evolution of backbone curves in the nonlinear parameter space,  $\alpha_1$  against  $\alpha_2$ , for a system with LA, i.e.  $m_1 = 1$ ,  $m_2 = 0.05$ ,  $k_1 = 1$  and  $k_2 = k_2^{\text{opt}} \approx 0.0454$ . The  $\alpha_1$  and  $\alpha_2$  values that lead to  $\psi_1 = 0$  and  $\psi_2 = 0$  are shown as a green dotted line and a purple dashed line, respectively. The panels around the main figure show backbone curves topologies for the nonlinear regions in terms of response frequency and displacement amplitude of the first mass. Panels (a, b, c, e, g, h, i, k) show these topologies in regions indicated by the solid-grey arrows. Panels (d, f, j, l) show the topologies corresponding to  $\alpha_1$  and  $\alpha_2$  axes, as indicated by the dash-dotted grey arrows. (Online version in colour.)

and

$$4(\omega_{n2}^2 - \Omega^2)U_2 + 3[\psi_5 U_2^3 + \psi_3 U_1^2 U_2 + p(\psi_1 U_1^3 + 3\psi_2 U_1 U_2^2)] = 0. \quad (3.19b)$$

Rearranging these two equations gives the frequency-amplitude relationships

$$\Omega^2 = \omega_{n1}^2 + \frac{3}{4}[\psi_4 U_1^3 + \psi_3 U_2^2 U_1 + p(\psi_2 U_2^3 + 3\psi_1 U_1^2 U_2)]U_1^{-1} \quad (3.20a)$$

and

$$0 = (-3p\psi_2 U_1^{-1})U_2^4 + 3(\psi_5 - \psi_3)U_2^3 + [9p(\psi_2 - \psi_1)U_1]U_2^2 + [4\omega_{n2}^2 - 4\omega_{n1}^2 + 3(\psi_3 - \psi_4)U_1^2]U_2 + 3p\psi_1 U_1^3, \quad (3.20b)$$

which may be solved to find the mixed-mode backbone curves.

Figure 8 presents the mixed-mode backbone curves of systems with linear parameters  $m_1 = 1$ ,  $m_2 = 0.05$ ,  $k_1 = 1$ ,  $k_2 = k_2^{\text{opt}} \approx 0.0454$  in the nonlinear parameter space  $\alpha_1$  against  $\alpha_2$ . Backbone curves on  $\psi_1 = 0$  and  $\psi_2 = 0$ , labelled in this figure, are the same as those in figures 7c, b,

respectively. This space is divided by the parameter axes  $\alpha_1 = 0$  and  $\alpha_2 = 0$  into the following four classes of system:

(i) **a hardening system (the first quadrant)**

Perturbing the nonlinear parameters clockwise from  $\psi_2 = 0$  breaks the perfect bifurcation on  $S_2$ , shown in figure 7b. The breaking of this bifurcation generates one isolated backbone curve,  $S_2^+$ , between two primary backbone curves,  $S_2^-$  and  $S_1^+$ ,<sup>4</sup> seen in figure 8a. Likewise, if nonlinear parameters are perturbed anticlockwise from  $\psi_2 = 0$ , the perfect bifurcation on  $S_2$  breaks in a different direction, resulting in one isolated backbone curve,  $S_2^-$ , below two primary backbone curves, depicted in figure 8b.

Further varying the nonlinear parameters in the anticlockwise direction towards  $\psi_1 = 0$ , the contribution of the second modal coordinate,  $U_2$ , to the mixed-mode, in-phase backbone curve,  $S_1^+$ , gradually decreases to zero. This results in a single-mode backbone curve  $S_1$ , seen from the evolution of backbone curves from figure 8b to 7c. Finally, perturbing anticlockwise from  $\psi_1 = 0$ , the  $U_2$  component of  $S_1$  increases, leading to a mixed-mode, anti-phase backbone curve  $S_1^-$ , as shown in figure 8c.

(ii) **a hardening structure with a softening attachment (the second quadrant)**

Further decreasing  $\alpha_2$  until  $\alpha_2 < 0$ , causes  $S_1^-$  to bend leftward, as depicted in figure 8e. Note that no isolated backbone curve is predicted for systems in the second quadrant.

(iii) **a softening system (the third quadrant)**

Crossing from the second quadrant into the third causes  $S_2^+$  to bend leftward, along with  $S_1^-$ . Continuing anticlockwise, from above  $\psi_2 = 0$  to below it, leads to a similar behaviour to the hardening system (the first quadrant) as it crosses  $\psi_1 = 0$ . The contribution from  $U_1$  to the mixed-mode, in-phase backbone curve  $S_2^+$  may gradually decrease, reaching zero at  $\psi_2 = 0$ , leading to a single-mode backbone curve  $S_2$ . The contribution then increases, resulting in a mixed-mode, anti-phase backbone curve  $S_2^-$ . Such behaviour is shown in figure 8g,h. Simultaneously, the isolated backbone curve,  $S_1^+$ , emerges from zero frequency and draws closer to the primary backbone curve  $S_1^-$ .

Further varying the nonlinear parameters towards  $\psi_1 = 0$ , the isolated and primary backbone curves,  $S_1^+$  and  $S_1^-$ , merge into a single-mode backbone curve,  $S_1$ , with a perfect bifurcation. Anticlockwise of  $\psi_1 = 0$ , the perfect bifurcation breaks and generates an isolated backbone curve,  $S_1^-$ , below two primary backbone curves,  $S_1^+$  and  $S_2^-$ , shown in figure 8i.

(iv) **a softening structure with a hardening attachment (the fourth quadrant)**

Crossing from the third to the fourth quadrant leads to the disappearance of the isolated backbone curve,  $S_1^-$ , at zero frequency, as shown in figure 8i,j. Additionally, the mixed-mode backbone curve,  $S_2^-$ , bends rightward, shown in figure 8j,k.

For further demonstration of the evolution of backbone curves in nonlinear parameter space, see the video, *Evolution of backbone curves.avi*, provided as electronic supplementary material.

From figure 8, it can be seen that the hardening systems (the first quadrant) and softening systems (the third quadrant) share the following features:

- (i) **a change of contribution of, and phase relationship between, two modal coordinates**, from being in-phase, to single-mode, and then to anti-phase, or vice versa, when crossing  $\psi_1 = 0$  and  $\psi_2 = 0$ ;
- (ii) **the emergence and breaking of a perfect bifurcation** on  $S_2$  for a hardening system when crossing  $\psi_2 = 0$ , and on  $S_1$  for a softening system when crossing  $\psi_1 = 0$ .

The perfect bifurcations denote critical conditions, perturbing from which leads to the onset of isolated backbone curves. These conditions are defined by relationships (3.17a,b) and thus

<sup>4</sup>Note that in other projections, such as  $\Omega$  against  $X_2$ , the relative amplitudes of these backbone curves may differ.

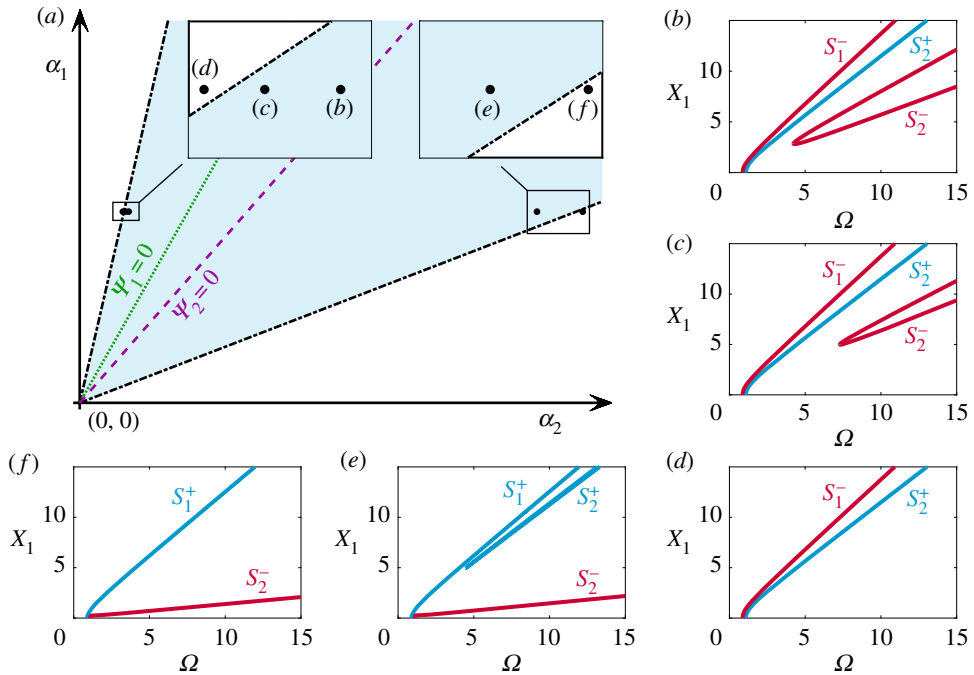


**Figure 9.** Two additional topological boundaries for the existence of isolated backbone curves. (a) The first quadrant of figure 8, along with two additional boundaries, shown as dash-dotted black lines, differentiating between regions with and without isolated backbone curves. Panels (b), . . . , (f) are backbone curves of systems represented by black dots in Panel (a) for a system with  $\alpha_1 = 1$  and varied  $\alpha_2$ . (Online version in colour.)

represent the boundaries for the existence of isolated backbone curves. The following section explores additional boundaries that may exist.

## 4. Additional topological boundaries

As described in §3b, a perturbation from  $\psi_2 = 0$  breaks the perfect bifurcation on  $S_2$ , for a hardening system, and results in an isolated backbone curve, shown in figures 7b and 8a,b. Further deviation may cause the isolated backbone curve to move toward higher frequency and larger amplitude, as depicted in figure 9b,c, which are corresponding to systems on points labelled (b) and (c), respectively in figure 9(a); eventually, the isolated backbone curve may undergo swift change from finite frequency and amplitude to infinite values. One example of this change is depicted in figure 9b–d. The isolated backbone curve first increases in frequency and amplitude at a limited rate, seen from figure 9b,c as  $\alpha_2$  changes from  $7.5 \times 10^{-4}$  to  $7.0 \times 10^{-4}$ . It then shifts to infinite frequency and amplitude as  $\alpha_2$  approaches a critical value of approximately  $6.76 \times 10^{-4}$ , shown in figure 9d. This corresponds to the vanishing (or emergence, if  $\alpha_2$  is increased) of an isolated backbone curve, and this critical value defines another topological difference in backbone curves, i.e. systems with and without an isolated backbone curve.

To find the conditions defining such boundaries in nonlinear parameter space, one can trace the isolated backbone curve to seek conditions for its existence. It is observed that the isolated backbone curve vanishes when the amplitude of the minimum frequency solution becomes infinite; hence, the conditions that lead to this case are investigated here.<sup>5</sup> Since the minimum frequency solution is related to a multiple root of amplitude for the frequency–amplitude

<sup>5</sup>There may be other conditions that allow isolated backbone curves to vanish/emerge; however, this particular case is investigated here as an example of such behaviour, rather than as an exhaustive study.



equations (3.20), one can refer to the zero discriminant of the amplitude equation (3.20*b*) to trace the multiple root. The zero discriminant of the quartic equation (3.20*b*) is a sixth-order polynomial equation with respect to  $U_1$ , and it can be written as

$$\text{Disc}_{U_2} = 0: \quad f_6 U_1^6 + f_5 U_1^5 + f_4 U_1^4 + f_3 U_1^3 + f_2 U_1^2 + f_1 U_1 + f_0 = 0, \quad (4.1)$$

where  $f_6$  is a function of nonlinear parameters, written as

$$f_6 = g_1 \alpha_1^6 + g_2 \alpha_1^5 \alpha_2 + g_3 \alpha_1^4 \alpha_2^2 + g_4 \alpha_1^3 \alpha_2^3 + g_5 \alpha_1^2 \alpha_2^4 + g_6 \alpha_1 \alpha_2^5 + g_7 \alpha_2^6, \quad (4.2)$$

and where coefficients  $g_1, \dots, g_7$  are determined by the underlying linear system, some of which are given in appendix B. Note that  $f_0, \dots, f_5, g_1, g_2, g_6$  and  $g_7$  are not provided as they are not required for the following derivations.

As the isolated backbone curve reaches the vanishing point, it has infinite amplitude; thus, letting  $U_1 \rightarrow \infty$ , gives

$$\text{Disc}_{U_2} \approx f_6 = 0. \quad (4.3)$$

After some algebraic manipulation, one can find coefficients  $g_1$  and  $g_7$  have factors  $(p-1)^2(p+1)^2$ , while coefficients  $g_2$  and  $g_6$  have factors  $(p-1)(p+1)$ . Recalling that  $p = \pm 1$ , defined in expression (3.18), it follows that  $g_1 = g_7 = g_2 = g_6 = 0$ , and equation (4.3) can be further simplified to give

$$f_6 = \alpha_1^2 \alpha_2^2 (g_3 \alpha_1^2 + g_4 \alpha_1 \alpha_2 + g_5 \alpha_2^2) = 0. \quad (4.4)$$

Two non-zero solutions for  $\alpha_2$  are

$$\alpha_2 = \frac{-g_4 \pm \sqrt{g_4^2 - 4g_5g_3}}{2g_5} \alpha_1. \quad (4.5)$$

Likewise, if frequency–amplitude relationships (3.20) are rearranged to give a quartic amplitude equation with respect to  $U_1$  rather than in  $U_2$ , as currently, one can find same expression as (4.5) by following the procedure demonstrated above. This means  $U_1$  and  $U_2$  will shift to infinity simultaneously on the critical conditions described by expression (4.5). As  $\Omega$  is explicitly determined by equation (3.20*a*), it will also shift to infinity when  $U_1 \rightarrow \infty$  and  $U_2 \rightarrow \infty$ .

Equation (4.5) represents conditions between  $\alpha_1$  and  $\alpha_2$  when the isolated backbone curve has infinite frequency and amplitude. This allows the first quadrant in figure 8, i.e. the hardening system, to be further divided into additional regions, as shown in figure 9*a*. The new regions anticlockwise of  $\Psi_1 = 0$  describe:

- (i) the shaded area anticlockwise of  $\Psi_1 = 0$ : two primary backbone curves,  $S_1^-$  and  $S_2^+$ , with one isolated backbone curve,  $S_2^-$ , below those two—shown in figure 9*b,c*;
- (ii) the unshaded area anticlockwise of  $\Psi_1 = 0$ : two primary backbone curves,  $S_1^-$  and  $S_2^+$ , without an isolated backbone curve—depicted in figure 9*d*.

The new regions clockwise of  $\Psi_2 = 0$  describe:

- (i) the shaded area clockwise of  $\Psi_2 = 0$ : two primary backbone curves,  $S_1^+$  and  $S_2^-$ , with one isolated backbone curve,  $S_2^+$ , between those two—shown in figure 9*e*;
- (ii) the unshaded area clockwise of  $\Psi_2 = 0$ : two primary backbone curves,  $S_1^+$  and  $S_2^-$ , without an isolated backbone curve—depicted in figure 9*f*.

In summary, expressions (3.17*a,b*), combined with conditions (3.15), are boundaries for the existence of a perfect bifurcation for a hardening and a softening system, respectively, perturbing from which the bifurcation breaks and an isolated backbone curve emerges. Expressions (4.5) describe the other boundaries at which isolated backbone curves may vanish or emerge from infinite frequency and amplitude. The shaded area in figure 9*a* highlights the region in which an isolated backbone curve can exist.

## 5. Conclusion

Isolated backbone curves can be related to isolated forced responses, which can have a significant negative impact on the performance of nonlinear engineering systems. This paper has investigated the conditions for the existence of isolated backbone curves of a two-mode system with cubic nonlinearities and a 1:1 resonance. The concept of *dynamic symmetry* has been defined as the case where a system exhibits two single-mode backbone curves with one perfect bifurcation. By breaking the symmetry of a simple example system, we have found that dynamic symmetry is still obtainable when the system is asymmetric. This highlights that an asymmetric system may exhibit dynamic behaviour that is equivalent to that of a symmetric system. A specific two-mode asymmetric system, composed of a primary structure and an NLTMD, was then considered, and an analytical approach was used to demonstrate that dynamic symmetry may only be achieved when the linear parameters obey specific relationships. After optimizing the linear parameters for vibration suppression performance, we have demonstrated analytical methods that allow the nonlinear parameter space to be divided into several regions, within which backbone curves present similar topological features. The boundaries of these regions define conditions for the existence of the isolated backbone curves. We have then demonstrated how these regions can be further refined by considering whether the isolated backbone curves can exist for finite amplitudes and frequencies.

The methodology used in this paper is based on a general two-mode model with cubic nonlinearities and a 1:1 internal resonance. While specific example systems have been considered, the approach used may be generalized to similar systems. This allows the existence of isolated backbone curves to be determined more rigorously when designing nonlinear systems.

**Data accessibility.** This article has no additional data.

**Authors' contributions.** D.H. led the development of the work, with supervisory support from T.L.H. and S.A.N. All authors contributed to the preparation of the manuscript.

**Competing interests.** We declare we have no competing interests.

**Funding.** S.A.N. is supported by the EPSRC (grant no. EP/R006768/1) and D.H. is supported by a scholarship from the CSC.

**Acknowledgements.** We gratefully acknowledge the financial support of the EPSRC and CSC.

## Appendix A. Modal analysis for the two-mass oscillator in §2

The equation of motion of the system shown in figure 1 is written as

$$\mathbf{M}\ddot{\mathbf{x}} + \mathbf{K}\mathbf{x} + \mathbf{N}_{\mathbf{x}} = \mathbf{0}, \quad (\text{A } 1)$$

where  $\mathbf{M}$  and  $\mathbf{K}$  are mass and linear stiffness matrices, respectively,  $\mathbf{N}_{\mathbf{x}}$  is a vector of nonlinear stiffness terms, and  $\mathbf{x}$  is a vector representing physical displacements. They are written

$$\mathbf{M} = \begin{bmatrix} m_1 & 0 \\ 0 & m_2 \end{bmatrix}, \quad \mathbf{K} = \begin{bmatrix} k_1 + k_2 & -k_2 \\ -k_2 & k_2 + k_3 \end{bmatrix} \quad (\text{A } 2)$$

and

$$\mathbf{N}_{\mathbf{x}} = \begin{pmatrix} \alpha_1 x_1^3 + \alpha_2 (x_1 - x_2)^3 \\ \alpha_2 (x_2 - x_1)^3 + \alpha_3 x_2^3 \end{pmatrix}, \quad \mathbf{x} = \begin{pmatrix} x_1 \\ x_2 \end{pmatrix}.$$

The system is translated into linear modal space by substituting  $\mathbf{x} = \boldsymbol{\Phi}\mathbf{q}$  into equations (A 1), where  $\boldsymbol{\Phi}$  is the linear modeshape matrix, which is written

$$\boldsymbol{\Phi} = \begin{bmatrix} \phi_{11} & \phi_{12} \\ \phi_{21} & \phi_{22} \end{bmatrix}. \quad (\text{A } 3)$$

Further multiplying both sides by  $\boldsymbol{\Phi}^T$ , the equations of motion can be obtained as

$$\boldsymbol{\Phi}^T \mathbf{M} \boldsymbol{\Phi} \ddot{\mathbf{q}} + \boldsymbol{\Phi}^T \mathbf{K} \boldsymbol{\Phi} \mathbf{q} + \mathbf{N}_{\mathbf{q}} = \mathbf{0} \quad (\text{A } 4)$$

where  $\mathbf{N}_q = \Phi^T \mathbf{N}_x(\Phi \mathbf{q})$  and  $\Phi^T \mathbf{M} \Phi = \mathbf{I}$ . As can be seen, after the linear modal transform, one can obtain the equations of motion in the same form as equations (2.2) with

$$\left. \begin{aligned} \Psi_1 &= \phi_{11}^3 \phi_{12} \alpha_1 + (\phi_{11} - \phi_{21})^3 (\phi_{12} - \phi_{22}) \alpha_2 + \phi_{21}^3 \phi_{22} \alpha_3, \\ \Psi_2 &= \phi_{11} \phi_{12}^3 \alpha_1 + (\phi_{11} - \phi_{21}) (\phi_{12} - \phi_{22})^3 \alpha_2 + \phi_{21} \phi_{22}^3 \alpha_3, \\ \Psi_3 &= 3 \left[ \phi_{11}^2 \phi_{12}^2 \alpha_1 + (\phi_{11} - \phi_{21})^2 (\phi_{12} - \phi_{22})^2 \alpha_2 + \phi_{21}^2 \phi_{22}^2 \alpha_3 \right], \\ \Psi_4 &= \phi_{11}^4 \alpha_1 + (\phi_{11} - \phi_{21})^4 \alpha_2 + \phi_{21}^4 \alpha_3 \\ \Psi_5 &= \phi_{12}^4 \alpha_1 + (\phi_{12} - \phi_{22})^4 \alpha_2 + \phi_{22}^4 \alpha_3. \end{aligned} \right\} \quad (\text{A } 5)$$

and

To interpret the modeshape elements  $\phi_{ij}$  by physical parameters, the linear modal analysis is then carried out by finding the eigenvalues and eigenvectors of  $\mathbf{M}^{-1} \mathbf{K}$ , leading to

$$\omega_{ni}^2 = \frac{[(k_2 + k_3)/m_2 + (k_1 + k_2)/m_1] \pm \sqrt{[(k_2 + k_3)/m_2 - (k_1 + k_2)/m_1]^2 + 4(k_2/m_1)(k_2/m_2)}}{2}, \quad (\text{A } 6)$$

and

$$\phi_{11}^2 = \frac{k_2^2}{(k_1 + k_2 - m_1 \omega_{n1}^2)^2 m_2 + m_1 k_2^2}, \quad \phi_{12}^2 = \frac{k_2^2}{(k_1 + k_2 - m_1 \omega_{n2}^2)^2 m_2 + m_1 k_2^2} \quad (\text{A } 7a)$$

and

$$\phi_{21}^2 = \frac{(k_1 + k_2 - m_1 \omega_{n1}^2)^2}{(k_1 + k_2 - m_1 \omega_{n1}^2)^2 m_2 + m_1 k_2^2}, \quad \phi_{22}^2 = \frac{(k_1 + k_2 - m_1 \omega_{n2}^2)^2}{(k_1 + k_2 - m_1 \omega_{n2}^2)^2 m_2 + m_1 k_2^2}. \quad (\text{A } 7b)$$

For the system shown in figure 5 with  $\Psi_1 = 0$  and  $\Psi_2 = 0$ , it satisfies parameter conditions described in equations (3.6) and (3.7). The modeshapes in expressions (A 7) can be further simplified as

$$\phi_{11}^2 = \frac{1}{2m_1 (1 + \mu + \sqrt{(1 + \mu)/\mu\mu})}, \quad \phi_{12}^2 = \frac{1}{2m_1 (1 + \mu - \sqrt{(1 + \mu)/\mu\mu})} \quad (\text{A } 8a)$$

and

$$\phi_{21}^2 = \frac{(\sqrt{(1 + \mu)/\mu} + 1)^2}{2m_1 (1 + \mu + \sqrt{(1 + \mu)/\mu\mu})}, \quad \phi_{22}^2 = \frac{(\sqrt{(1 + \mu)/\mu} - 1)^2}{2m_1 (1 + \mu - \sqrt{(1 + \mu)/\mu\mu})}. \quad (\text{A } 8b)$$

where  $\mu = m_1/m_2$ , which is the mass ratio.

For the specific system, shown schematically in figure 1, with symmetric linear parameters, i.e.  $m_1 = m_2$  and  $k_1 = k_3$ , the modeshape elements satisfy  $\phi_{11} = \phi_{12} = \phi_{21} = -\phi_{22}$ , obtained from expressions (A 7). Thus,  $\Psi_1$  and  $\Psi_2$ , expressed in equations (A 5), can be reduced to

$$\Psi_1 = \Psi_2 = \phi_{11}^4 (\alpha_1 - \alpha_3). \quad (\text{A } 9)$$

As discussed in §2, obtaining dynamic symmetry requires two single-mode solutions, i.e. satisfying  $\Psi_1 = 0$  and  $\Psi_2 = 0$ . As seen from equations (A 9),  $\Psi_1 = 0$  and  $\Psi_2 = 0$  can only be satisfied when  $\alpha_1 = \alpha_3$ , which means having symmetric nonlinear parameters. In summary, to obtain dynamic symmetry for a system with linear symmetry requires nonlinear symmetry.

## Appendix B. List of coefficients

$$g_3 = -19683 \left( \phi_{11}^2 + \phi_{12}^2 \right)^4 \left( \phi_{11} \delta_{11} + \phi_{12} \delta_{12} \right)^2 \left( \phi_{11} \delta_{12} - \phi_{12} \delta_{11} \right)^6, \quad (\text{B1})$$

$$g_5 = -19683 \left( \delta_{11}^2 + \delta_{12}^2 \right)^4 \left( \phi_{11} \delta_{11} + \phi_{12} \delta_{12} \right)^2 \left( \phi_{11} \delta_{12} - \phi_{12} \delta_{11} \right)^6 \quad (\text{B2})$$

$$\text{and } g_4 = -19683P \left( \phi_{11} \delta_{12} - \phi_{12} \delta_{11} \right)^6, \quad (\text{B3})$$

where

$$\begin{aligned} P = & \left( 2\phi_{11}^6 - 8\phi_{11}^4\phi_{12}^2 - \frac{2}{3}\phi_{11}^2\phi_{12}^4 - \frac{4}{27}\phi_{12}^6 \right) \delta_{11}^6 + \left( 2\phi_{12}^6 - 8\phi_{11}^2\phi_{12}^4 - \frac{2}{3}\phi_{11}^4\phi_{12}^2 - \frac{4}{27}\phi_{11}^6 \right) \delta_{12}^6 \\ & + \left( 28\phi_{11}^5\phi_{12} - \frac{88}{3}\phi_{11}^3\phi_{12}^3 - \frac{4}{9}\phi_{11}\phi_{12}^5 \right) \delta_{11}^5\delta_{12} + \left( 28\phi_{11}\phi_{12}^5 - \frac{88}{3}\phi_{11}^3\phi_{12}^3 - \frac{4}{9}\phi_{11}^5\phi_{12} \right) \delta_{11}\delta_{12}^5 \\ & + \left( -8\phi_{11}^6 + 90\phi_{11}^4\phi_{12}^2 - \frac{404}{9}\phi_{11}^2\phi_{12}^4 - \frac{2}{3}\phi_{12}^6 \right) \delta_{11}^4\delta_{12}^2 \\ & + \left( -8\phi_{12}^6 + 90\phi_{11}^2\phi_{12}^4 - \frac{404}{9}\phi_{11}^4\phi_{12}^2 - \frac{2}{3}\phi_{11}^6 \right) \delta_{11}^2\delta_{12}^4 \\ & + \left( -\frac{88}{3}\phi_{11}^5\phi_{12} + \frac{3536}{27}\phi_{11}^3\phi_{12}^3 - \frac{88}{3}\phi_{12}^5\phi_{11} \right) \delta_{11}^3\delta_{12}^3, \end{aligned} \quad (\text{B4})$$

and where  $\delta_{11} = \phi_{11} - \phi_{21}$  and  $\delta_{12} = \phi_{12} - \phi_{22}$ .

## References

1. Cartmell M. 1990 *Introduction to linear, parametric, and nonlinear vibrations*. Berlin, Germany: Chapman and Hall.
2. Jezequel L, Lamarque CH. 1991 Analysis of non-linear dynamical systems by the normal form theory. *J. Sound Vib.* **149**, 429–459. (doi:10.1016/0022-460X(91)90446-Q)
3. Thomsen JJ. 1994 *Stability, instability and chaos: an introduction to the theory of nonlinear differential equations*. Cambridge Texts in Applied Mathematics. Cambridge, UK: Cambridge University Press.
4. Wagg DJ, Neild SA. 2009 *Nonlinear vibration with control*. Berlin, Germany: Springer.
5. Kerschen G, Peeters M, Golinval JC, Vakakis AF. 2009 Nonlinear normal modes, part I: a useful framework for the structural dynamicist. *Mech. Syst. Signal Process.* **23**, 170–194. (doi:10.1016/j.ymsp.2008.04.002)
6. Pierre C, Jiang D, Shaw S. 2006 Nonlinear normal modes and their application in structural dynamics. *Math. Probl. Eng.* **2006**, 15. (doi:10.1155/MPE/2006/10847) Article ID 10847
7. Vakakis AF. 2001 Inducing passive nonlinear energy sinks in vibrating systems. *J. Vib. Acoust.* **123**, 324–332. (doi:10.1115/1.1368883)
8. Kerschen G, Kowtko JJ, McFarland DM, Bergman LA, Vakakis AF. 2007 Theoretical and experimental study of multimodal targeted energy transfer in a system of coupled oscillators. *Nonlinear Dyn.* **47**, 285–309. (doi:10.1007/s11071-006-9073-5)
9. Antonio D, Zanette DH, López D. 2012 Frequency stabilization in nonlinear micromechanical oscillators. *Nat. Commun.* **3**, 806. (doi:10.1038/ncomms1813)
10. Febbo M, Machado SP. 2013 Nonlinear dynamic vibration absorbers with a saturation. *J. Sound Vib.* **332**, 1465–1483. (doi:10.1016/j.jsv.2012.11.025)
11. Carpineto N, Lacarbonara W, Vestroni F. 2014 Hysteretic tuned mass dampers for structural vibration mitigation. *J. Sound Vib.* **333**, 1302–1318. (doi:10.1016/j.jsv.2013.10.010)
12. Barton DAW, Burrow SG, Clare LR. 2010 Energy harvesting from vibrations with a nonlinear oscillator. *J. Vib. Acoust.* **132**, 021009. (doi:10.1115/1.4000809)
13. Green PL, Worden K, Atallah K, Sims ND. 2012 The benefits of Duffing-type nonlinearities and electrical optimisation of a mono-stable energy harvester under white Gaussian excitations. *J. Sound Vib.* **331**, 4504–4517. (doi:10.1016/j.jsv.2012.04.035)
14. Gourdon E, Alexander NA, Taylor CA, Lamarque CH, Pernot S. 2007 Nonlinear energy pumping under transient forcing with strongly nonlinear coupling: theoretical and experimental results. *J. Sound Vib.* **300**, 522–551. (doi:10.1016/j.jsv.2006.06.074)

15. Vakakis AF, Gendelman OV, Bergman LA, McFarland DM, Kerschen G, Lee YS. 2009 *Nonlinear targeted energy transfer in mechanical and structural systems*. Dordrecht, The Netherlands: Springer.
16. Habib G, Detroux T, Vigi   R, Kerschen G. 2015 Nonlinear generalization of Den Hartog's equal-peak method. *Mech. Syst. Signal Process.* **52**–**53**, 17–28. (doi:10.1016/j.ymssp.2014.08.009)
17. Gatti G. 2018 Fundamental insight on the performance of a nonlinear tuned mass damper. *Meccanica* **53**, 111–123. (doi:10.1007/s11012-017-0723-0)
18. Den Hartog JP. 1956 *Mechanical vibrations*, 4th edn. New York, NY: McGraw-Hill.
19. Malher A, Touz   C, Doar   O, Habib G, Kerschen G. 2017 Flutter control of a two-degrees-of-freedom airfoil using a nonlinear tuned vibration absorber. *J. Comput. Nonlinear Dyn.* **12**, 051016. (doi:10.1115/1.4036420)
20. Habib G, Kerschen G. 2015 Suppression of limit cycle oscillations using the nonlinear tuned vibration absorber. *Proc. R. Soc. A* **471**, 20140976. (doi:10.1098/rspa.2014.0976)
21. Alexander NA, Schilder F. 2009 Exploring the performance of a nonlinear tuned mass damper. *J. Sound Vib.* **319**, 445–462. (doi:10.1016/j.jsv.2008.05.018)
22. Gatti G, Brennan M. 2011 On the effects of system parameters on the response of a harmonically excited system consisting of weakly coupled nonlinear and linear oscillators. *J. Sound Vib.* **330**, 4538–4550. (doi:10.1016/j.jsv.2011.04.006)
23. Detroux T, Habib G, Masset L, Kerschen G. 2015 Performance, robustness and sensitivity analysis of the nonlinear tuned vibration absorber. *Mech. Syst. Signal Process.* **60**–**61**, 799–809. (doi:10.1016/j.ymssp.2015.01.035)
24. Abramson HN. 1955 Response curves for a system with softening restoring force. *J. Appl. Mech.* **22**, 434–435.
25. Duan C, Singh R. 2007 Isolated sub-harmonic resonance branch in the frequency response of an oscillator with slight asymmetry in the clearance. *J. Sound Vib.* **314**, 12–18. (doi:10.1016/j.jsv.2007.12.040)
26. Misra S, Dankowicz H, Paul MR. 2010 Degenerate discontinuity-induced bifurcations in tapping-mode atomic-force microscopy. *Physica D* **239**, 33–43. (doi:10.1016/j.physd.2009.10.001)
27. Nayfeh AH, Mook DT. 1995 *Nonlinear oscillations, physics textbook*. Weinheim, Germany: Wiley.
28. DiBerardino LA, Dankowicz H. 2013 Accounting for nonlinearities in open-loop protocols for symmetry fault compensation. *J. Comput. Nonlinear Dyn.* **9**, 021002. (doi:10.1115/1.4025193)
29. Hill TL, Neild SA, Cammarano A. 2016 An analytical approach for detecting isolated periodic solution branches in weakly nonlinear structures. *J. Sound Vib.* **379**, 150–165. (doi:10.1016/j.jsv.2016.05.030)
30. Kuether RJ, Renson L, Detroux T, Grappasonni C, Kerschen G, Allen MS. 2015 Nonlinear normal modes, modal interactions and isolated resonance curves. *J. Sound Vib.* **351**, 299–310. (doi:10.1016/j.jsv.2015.04.035)
31. Grenat C, Baguet S, Lamarque CH, Dufour R. 2019 A multi-parametric recursive continuation method for nonlinear dynamical systems. *Mech. Syst. Signal Process.* **127**, 276–289. (doi:10.1016/j.ymssp.2019.03.011)
32. Habib G, Cirillo G, Kerschen G. 2017 Uncovering detached resonance curves in single-degree-of-freedom systems. *Procedia Eng.* **199**, 649–656. (doi:10.1016/j.proeng.2017.09.116)
33. Cirillo GI, Habib G, Kerschen G, Sepulchre R. 2017 Analysis and design of nonlinear resonances via singularity theory. *J. Sound Vib.* **392**, 295–306. (doi:10.1016/j.jsv.2016.12.044)
34. Habib G, Cirillo GI, Kerschen G. 2018 Isolated resonances and nonlinear damping. *Nonlinear Dyn.* **93**, 979–994. (doi:10.1007/s11071-018-4240-z)
35. No  l JP, Detroux T, Masset L, Kerschen G, Virgin LN. 2015 Isolated response curves in a base-excited, two-degree-of-freedom, nonlinear system. In *Volume 6: 11th International Conference on Multibody Systems, Nonlinear Dynamics, and Control; ASME 2015 Int. Design Engineering Technical Conferences and Computers and Information in Engineering Conf.*, Boston, MA, 2–5 August. New York, NY: American Society of Mechanical Engineers.
36. Renson L, Barton DAW, Neild SA. 2019 Application of control-based continuation to a nonlinear system with harmonically coupled modes. In *Nonlinear dynamics* (ed. G Kerschen), vol. 1, pp. 315–316 Cham, Switzerland: Springer International Publishing.
37. Vakakis AF. 1997 Non-linear normal modes (NNMs) and their applications in vibration theory: an overview. *Mech. Syst. Signal Process.* **11**, 3–22. (doi:10.1006/mssp.1996.9999)

38. Hill TL, Cammarano A, Neild SA, Wagg DJ. 2015 Interpreting the forced responses of a two-degree-of-freedom nonlinear oscillator using backbone curves. *J. Sound Vib.* **349**, 276–288. (doi:10.1016/j.jsv.2015.03.030)
39. Ehrhardt DA, Hill TL, Neild SA. 2019 Experimentally measuring an isolated branch of Nonlinear normal modes. *J. Sound Vib.* **457**, 213–226. (doi:10.1016/j.jsv.2019.06.006)
40. Rand RH. 2005 *Lecture notes on nonlinear vibrations*. Ithaca, NY: Department of Theoretical and Applied Mechanics, Cornell University.
41. Cammarano A, Hill TL, Neild SA, Wagg DJ. 2014 Bifurcations of backbone curves for systems of coupled nonlinear two mass oscillator. *Nonlinear Dyn.* **77**, 311–320. (doi:10.1007/s11071-014-1295-3)
42. Muravyov AA, Rizzi SA. 2003 Determination of nonlinear stiffness with application to random vibration of geometrically nonlinear structures. *Comput. Struct.* **81**, 1513–1523. (doi:10.1016/S0045-7949(03)00145-7)
43. Tartaruga I, Elliott A, Hill TL, Neild SA, Cammarano A. 2019 The effect of nonlinear cross-coupling on reduced-order modelling. *Int. J. Non-Linear Mech.* **116**, 7–17. (doi:10.1016/j.ijnonlinmec.2019.05.006)
44. Neild SA, Wagg DJ. 2011 Applying the method of normal forms to second-order nonlinear vibration problems. *Proc. R. Soc. A* **467**, 1141–1163. (doi:10.1098/rspa.2010.0270)
45. Lacarbonara W. 2013 *Nonlinear normal modes for damage detection*. New York, NY: Springer.
46. Hill TL, Cammarano A, Neild SA, Wagg DJ. 2015 Out-of-unison resonance in weakly nonlinear coupled oscillators. *Proc. R. Soc. A* **471**, 20140659. (doi:10.1098/rspa.2014.0659)
47. Asami T, Nishihara O. 2003 Closed-form exact solution to  $H_\infty$  optimization of dynamic vibration absorbers (application to different transfer functions and damping systems). *J. Vib. Acoust.* **125**, 398–405. (doi:10.1115/1.1569514)